

**ThesisTitle**

by

**Daniel C. Cole**

Other Degrees

A thesis submitted to the  
Faculty of the Graduate School of the  
University of Colorado in partial fulfillment  
of the requirements for the degree of  
Doctor of Philosophy  
Physics Physics  
2018

This thesis entitled:  
ThesisTitle  
written by Daniel C. Cole  
has been approved for the Physics Physics

---

Reader1

---

Reader2

Date \_\_\_\_\_

The final copy of this thesis has been examined by the signatories, and we find that both the content and the form meet acceptable presentation standards of scholarly work in the above mentioned discipline.

Cole, Daniel C. (Ph.D., Physics)

ThesisTitle

Thesis directed by Dr. Scott A. Diddams

Optical frequency combs have revolutionized precision metrology by enabling measurements of optical frequencies, with implications both for fundamental scientific questions and for applications such as fast, broadband spectroscopy. In this thesis, I describe the development of comb generation platforms with smaller footprints and higher repetition rates, with the ultimate goal of bringing frequency combs to new applications in a chip-integrated package. I present two new types of frequency combs: electro-optic modulation (EOM) combs and Kerr-microresonator-based frequency combs (microcombs). First I describe the EOM comb scheme and, in particular, techniques for mitigating noise in the comb generation process, and I present the results of a proof-of-principle metrology experiment and some possible applications. Then I discuss developments in microcomb technology. I present novel ‘soliton crystal’ states, which have highly structured ‘fingerprint’ optical spectra that correspond to ordered pulse trains exhibiting crystallographic defects. These pulse trains arise through interaction of the solitons with avoided mode-crossings in the resonator spectrum. Next, I describe the direct and deterministic generation of single microresonator solitons using a phase-modulated pump laser. This technique removes the dependence on initial conditions that was formerly a universal feature of these experiments, presenting a solution to a significant technical barrier to the practical application of microcombs. I also discuss generation of Kerr combs in the Fabry-Perot (FP) geometry. I introduce a nonlinear partial differential equation describing dynamics in an FP cavity and discuss the differences between the FP geometry and the ring cavity, which is the geometry used in previous Kerr-comb experiments. Finally, I discuss a technique for reducing the repetition rate of a high-repetition-rate frequency comb, which will be a necessary post-processing step for some applications. I conclude with a discussion of avenues for future research, including the chip-integration of Fabry-Perot Kerr resonators and the use of band-engineered photonic crystal cavities to further simplify soliton generation.

## Acknowledgements

The work in this thesis would not have been possible...

- Acknowledgement line 1
- Acknowledgement line 2

## Contents

<b>1</b>	<b>Soliton Crystals</b>	<b>1</b>
1.1	Spectral and temporal characteristics of soliton crystals . . . . .	1
1.2	Soliton crystal generation . . . . .	3
1.3	Mechanism of soliton crystallization . . . . .	4
1.3.1	Simulation of soliton crystals . . . . .	7
1.4	Case study: pair distribution function for a superstructured crystal . . . . .	8
1.5	Soliton crystal configuration space . . . . .	11
1.6	Time-domain measurements of soliton crystals . . . . .	15
<b>References</b>		<b>18</b>

## Figures

1.1	Spectral contrast of a soliton crystal . . . . .	3
1.2	Generation and characterization of a soliton crystal . . . . .	5
1.3	Stabilization and collapse of a soliton crystal . . . . .	8
1.4	Spectrum and waveform of a superstructured soliton crystal . . . . .	9
1.5	Simulated generation of a superstructured soliton crystal . . . . .	10
1.6	Pair distribution function for soliton crystal generation . . . . .	11
1.7	Taxonomy of soliton crystals . . . . .	14
1.8	Cross-correlation characterization of a soliton crystal . . . . .	17

# Chapter 1

## Soliton Crystals

This chapter presents results on the self-organization of ensembles of solitons in optical microring resonators. These results involve physics beyond the basic LLE model for Kerr-comb formation, as is described in Sec. 1.3. These experiments are performed using silica micro-rod [2] and micro-disk [39] resonators with  $\sim 25$  GHz and  $\sim 16.5$  GHz FSR, respectively, but the principle applies to any resonator that supports multiple transverse mode intensity profiles. We refer to these self-organized soliton ensembles as ‘soliton crystals,’ which extends an analogy to condensed-matter physics that has been made in other nonlinear-optical systems, including single-pass nonlinear fiber systems [40] and harmonically mode-locked fiber laser [41, 42], where a different mechanism for soliton crystallization that is based on two distinct timescales of the laser medium was identified [43]. Notably, the spatiotemporal chaos exhibited by Kerr combs was referred to as a ‘soliton gas’ in early studies of nonlinear dynamics in passive fiber-loop resonators [44–46].

### 1.1 Spectral and temporal characteristics of soliton crystals

Soliton crystals in Kerr resonators are soliton ensembles in which each soliton lies on a lattice site  $\theta_n = 2\pi n/N$  in the azimuthal co-moving frame, where  $N$  is a lattice parameter that arises from the fundamental physics of the system as described below and  $n$  indexes over the lattice sites. In a typical soliton crystal there are many more available lattice sites than solitons, so that a fraction of the lattice sites are occupied. In the frequency domain, the temporal ordering of pulses in a soliton crystal corresponds to a highly modulated optical spectrum that exhibits distinctive features.

We present plots illustrating the spectral and temporal characteristics of an example soliton crystal in Fig. 1.1. Fig. 1.1a shows an experimental measurement of a soliton crystal spectrum. This spectrum exhibits prominent comb modes similar to primary-comb lines, and underlying these primary-comb lines are single-FSR-spaced spectral lobes. We can understand this spectrum through the basic superposition principle of the electric field: The primary comb spectrum with spacing  $N \times f_{FSR}$  corresponds to a train of  $N$  uniformly spaced pulses in the resonator. To this pulse train we add an *out-of-phase* pulse  $S_-$  that coincides in time with one of the existing pulses—in the time domain this corresponds to the introduction of a vacancy into the pulse train, while in the frequency domain this corresponds to the addition (in the phase-sensitive field quantity) of the primary-comb spectrum and the spectrum of the single, out-of-phase soliton. We then add a second soliton  $S_+$  to the pulse train, this one *in phase* with the existing pulses and slightly temporally shifted from the vacancy. The time-domain result is a pulse train with one pulse displaced from its expected position based on uniform spacing. In the frequency domain, the positions of the pulses  $S_+$  and  $S_-$  correspond to different linear spectral phase shifts on each of their individual spectra; when these spectra are added together (in the phase-sensitive field quantity) the result is spectral interference that is periodic in frequency. This gives rise to the lobes beneath the primary-comb lines; the period (in frequency) of the interference is inversely proportional to the separation between the pulses  $S_+$  and  $S_-$  in time.

We illustrate this principle by plotting pulse trains exhibiting a shifted pulse in Fig. 1.1b, and show their calculated spectra in Fig. 1.1a. These pulse trains are not the result of LLE simulations—instead they are analytical approximations to soliton ensembles using Eq. ???. The pulse train shown in orange is composed of solitons pinned to sites on a lattice, and the pulse train shown in blue is obtained from this first pulse train by introducing a small random displacement to the position of each pulse. The effect of this small position jitter is apparent in the calculated spectra in Fig. 1.1a—the highly-distinctive spectral characteristics of the soliton crystal are eroded. In fact, it is a general property of the soliton-crystal spectra that we present in this chapter that the contrast and definition of the distinct spectral characteristics depends on the high precision with which the

do I have  
an equation  
for soliton  
ensembles?

pulses fall on the lattice sites.

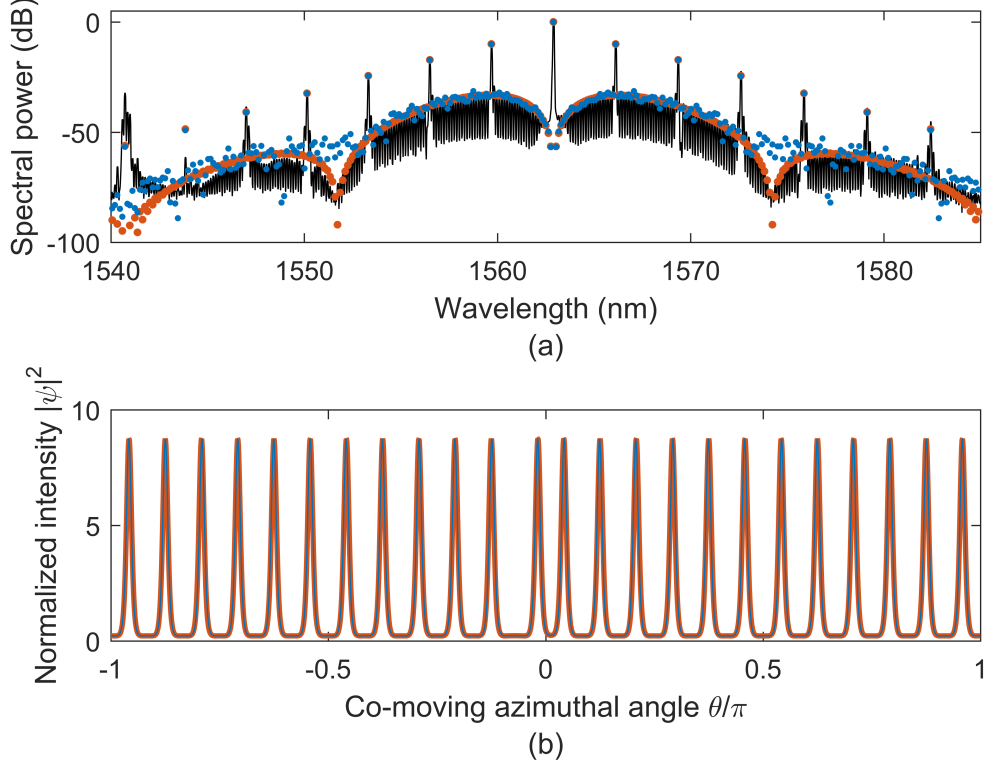


**Figure 1.1: Spectral contrast of a soliton crystal.** (a) Experimental measurement of a soliton-crystal spectrum (black), along with two approximations to the crystal's time-domain waveform as a superposition of solitons, according to Eq. ???. Shown in orange is the spectrum of an ensemble of solitons pinned to sites on a lattice with spacing  $2\pi/(7 \times 24)$ ; here the majority of the pulses are separated from their neighbors by seven lattice sites, but one pulse is displaced by two lattice sites from its expected position. Shown in blue is a calculation of the spectrum that results when random (uniformly distributed) jitter is imposed on the same pulse positions; the range of the jitter is  $\pm 3\%$  of the typical inter-soliton spacing  $2\pi/24$ . (b) Time-domain traces corresponding to the spectra shown in (a). There is no readily apparent difference between the positions of the pulses in two pulse trains because the magnitude of the imposed jitter is small.

## 1.2 Soliton crystal generation

Soliton crystals are characterized by stable, dense occupation of the resonator by soliton pulses, and this dense occupation comes with high circulating power relative to single solitons or few-soliton ensembles. This important fact allows soliton crystals to be generated with decreasing pump-laser frequency scans across the resonance that are adiabatic—slow enough that both the

resonator temperature and the state of the comb  $\psi$  are maintained at values<sup>1</sup> that correspond to the instantaneous  $\alpha$  and  $F^2$  parameters throughout the scan. We demonstrate generation of a soliton crystal in a slow scan in Fig. 1.2; it is useful to contrast this with the behavior exhibited in Fig. ??.

something  
about soli-  
ton steps  
here

### 1.3 Mechanism of soliton crystallization

The simulated time-domain waveforms we have considered so far are not stable in evolution under the LLE. For each, the observed width of the spectrum fixes the ratio between  $\alpha$  and  $\beta$ , as seen from Eq. ???. This ratio then fixes the temporal duration of the solitons, in turn determining the characteristic length of their interactions. When an attempt to simulate the crystal according to the LLE is made with parameters (e.g.  $F^2=3.7$ ,  $\alpha = 3.77$ , and  $\beta = -0.0054$  for the crystal in Fig. 1.2c and d) that give agreement with the measured width of the optical spectrum, it is found that pair-wise attractive interactions between solitons lead to collapse of the crystal.

A stabilization mechanism that goes beyond the physics of the LLE is responsible for the stability of this and other soliton crystals. The stabilization mechanism arises from avoided mode-crossings in the resonator spectrum. A ‘mode family’ corresponds to a set of circulating modes that have different azimuthal mode numbers but (approximately, neglecting wavelength-dependent effects) the same transverse spatial mode profile. As discussed in Sec. ??, some resonators support multiple mode families, each with its own free spectral range at a given wavelength. Although the modes in different families are in principle orthogonal, coupling between them can be provided by perturbations, for example by the coupling waveguide or tapered fiber used to drive the resonator. If a coupling exists between two modes that are sufficiently close in frequency, the frequencies of the modes become displaced from their frequencies in the absence of this coupling [47]. This affects Kerr-comb generation in the affected mode families, because the local detuning between the resonator modes and the Kerr-comb modes is changed as a result of the mode crossing. This comb-resonator detuning change may either enhance or inhibit nonlinear frequency conversion to the effected Kerr-

I don't like  
this para-  
graph and  
the following  
one

<sup>1</sup> This terminology is a bit imprecise when applied to chaotic Kerr-combs that evolve with time; in this case the chaos exhibits the same behavior at each point in the scan that would be expected if  $\alpha$  and  $F^2$  were held fixed.

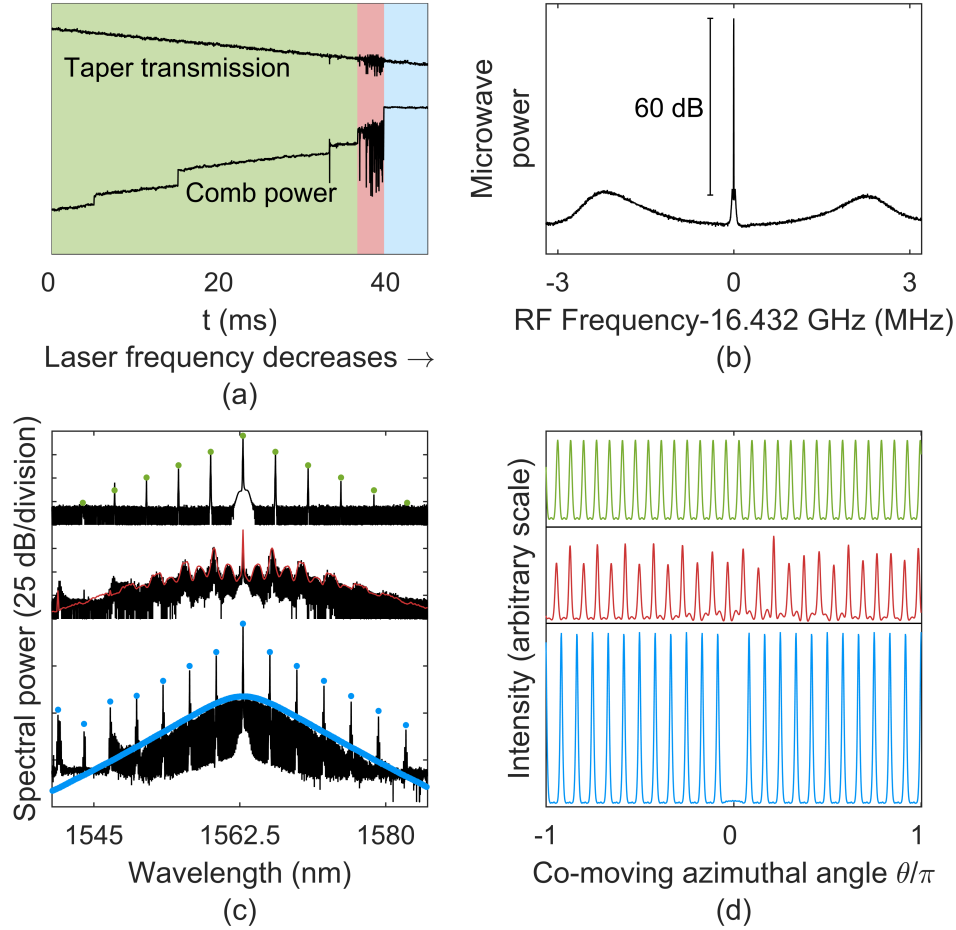


**Figure 1.2: Generation and characterization of a soliton crystal.** (a) Measurements of the power transmitted past the resonator ('Taper transmission') and this power with the pump frequency filtered out ('Comb power') during crystal generation with a scan that proceeds through primary-comb (green), chaotic (red), and soliton crystal (blue) regimes. The resonator's thermal response leads to the non-Lorentzian taper transmission profile, and the continuity of the taper transmission trace upon soliton crystal condensation indicates that the intracavity power of the soliton crystal is matched to the chaos that precedes it. (b) Narrow measured RF beat for the repetition rate of the soliton crystal is indicative of a coherent comb, in contrast with the chaotic state. (c) Progression of the optical spectrum through the scan, with experimental data (black) obtained by halting the scan at the appropriate point, and LLE simulations (with a perturbation as described in Sec. 1.3) in color. The simulated spectrum for the chaotic state shown in red is a time average. (d) Simulated time-domain traces corresponding to the simulated spectra in (c). The simulated intensity for the chaotic state is a snapshot. The soliton crystal shown in blue is a uniform pulse train with a single vacancy (see text).

comb modes, thereby changing the amplitude of these modes in the comb spectrum.

It has been reported that avoided mode crossings in the resonator spectrum can inhibit soliton generation in anomalous-dispersion resonators [29, 48], while they can facilitate the formation of

Kerr-combs in normal-dispersion resonators [49]. Here we are interested specifically in the impact of the avoided mode crossing on the waveform of a soliton. For simplicity, we focus on the case where a single comb mode with number  $\mu_x$  is affected by the mode crossing. When the change in the comb-resonator detuning increases the amplitude of mode  $\mu_x$  in the soliton's spectrum, the change to the time-domain waveform can be understood by considering this increase as the addition of extra CW light at the frequency  $\mu_x$ . This extra CW light exists throughout the cavity, and it leads the introduction of periodic intensity oscillations in the background on which the soliton rides as the new CW light beats against the existing background at the pump frequency. This new background wave in the cavity has a period of  $2\pi/\mu_x$  in the angular coordinate  $\theta$ .

other citations here

When several of these perturbed solitons co-propagate in a resonator, they interact through their extended waves and arrange themselves such that the waves constructively interfere. Each soliton then lies at the peak of a single extended background wave in the resonator, similar to predictions for bichromatically pumped Kerr combs [50]. Importantly, temporal separations between solitons are therefore required to be multiples of this wave's period, and the wave stabilizes the crystal against the attractive interactions discussed above. Furthermore, the wave's amplitude, and thus the strength of the crystal against perturbations, increases with the number of co-propagating perturbed solitons. Finally, we note that at least within the assumption of single-mode perturbation of the comb's spectrum, this interaction has infinite range.

We note that the mechanism observed here builds on previous reports of related phenomena. It has been shown that local interactions between cavity solitons can arise through decaying oscillatory tails [51], leading to the formation of small, locally ordered soliton molecules. Furthermore, it has been shown that the injection of an additional CW laser into a passive fiber-ring resonator can result in the generation of uniform distributions of solitons [52]. The mechanism we report here can be viewed as a variant of this CW-soliton interaction in which the 'injected' CW laser is provided by the effect of the mode crossing on the solitons' spectra.

We connect this discussion to the soliton-crystal spectrum presented in the bottom trace of Fig. 1.2c—this spectrum exhibits excess power near pump-referenced modes numbers  $\mu_{x,1} = 5 \times 24 = 120$

(1547 nm) and  $\mu_{\times,2} = 7 \times 24 = 168$  (1541 nm). Also visible is suppressed comb generation where the comb-resonator detuning has been increased. Here 24 FSR is the spacing of the prominent primary-comb lines.

### 1.3.1 Simulation of soliton crystals

To incorporate the stabilization mechanism described above into numerical simulations, we incorporate into the LLE a reduced comb-resonator detuning on a single mode  $\mu_{\times}$ . The mode-dependent comb-resonator detuning can be calculated as:

$$\alpha_{\mu} = -2(\Omega_0 - D_1 + \omega_{\mu})/\Delta\omega, \quad (1.1)$$

$$= \alpha - \beta\mu^2/2. \quad (1.2)$$

Here  $\Omega_0$  is the frequency of the pump laser,  $\omega_{\mu}$  is the set of cavity resonance frequencies referenced to the pumped mode, and  $D_1 = \partial\omega_{\mu}/\partial\mu|_{\mu=0}$  is the resonator's FSR at the pumped mode and is also assumed to be the Kerr-comb's repetition rate. The dispersion operator is applied in the frequency domain in numerical simulations of the LLE (see ??), which facilitates inclusion of  $\delta$ -function perturbations to the comb-resonator detuning as:

$$\alpha_{\mu} = \alpha - \beta\mu^2/2 + \Delta\alpha_{\mu}, \quad (1.3)$$

where

$$\Delta\alpha_{\mu} = 2(\omega_{\mu} - \omega_{\mu,0})/\Delta\omega \quad (1.4)$$

is the normalized change in the frequency of mode  $\mu$  from the expected frequency  $\omega_{\mu,0}$ .

We demonstrate the stabilization mechanism and the simulation method by presenting a simulation of the crystal in Fig. 1.2c. The simulation is shown in Fig. ???. This figure illustrates that, without the stabilization mechanism, the crystal will collapse. We note that a phenomenological application of coupled-mode theory [47] could be used to calculate the full perturbation to the soliton spectrum by the mode crossing, but we find that to explain the existence of this 23-soliton crystal and the apparently exact circumferential spacing of the pulses by  $2\pi/24$  radians, it is sufficient to incorporate into the LLE a reduced comb-resonator detuning on only mode 120 or on mode

168, where the excess power is largest. The crystal is then a steady-state solution of the resulting perturbed LLE.

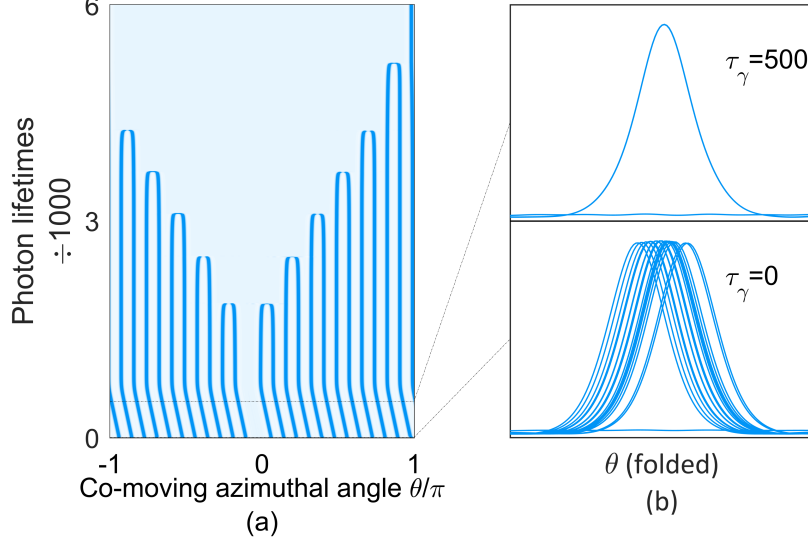


**Figure 1.3: Stabilization and collapse of a soliton crystal.** (a) Simulated evolution of the pulse train corresponding to the experimental crystal spectrum shown in Fig. 1.2c, starting from irregular pulse positions. For the first 500 photon lifetimes of the simulation, the propagation is governed by a perturbed LLE including reduced comb-resonator detuning on modes  $\mu_{x,1} = 120$  and  $\mu_{x,2} = 168$ . The soliton ensemble crystallizes within 10 seconds of initialization of the simulation, and then drifts within the co-rotating frame because the additional CW light on modes  $\mu_{x,1}$  and  $\mu_{times,2}$  correspond to traveling waves. The reduced comb-resonator detuning is removed smoothly from 500 to 1000 photon lifetimes, resulting in the destabilization of the crystal and pair-wise annihilation of the solitons. (b) Intracavity power with the azimuthal coordinate folded modulo  $2\pi/24$ , demonstrating the initial irregularity of the pulse positions and the crystallized pulse train after 500 photon lifetimes.

#### 1.4 Case study: pair distribution function for a superstructured crystal

We consider a second specific example of a soliton crystal. The measured optical spectrum for this crystal is shown in Fig. 1.4a. This crystal exhibits superstructure—the soliton pulse train is nearly periodic in a small unit cell but is modulated with a larger periodicity. This results from the frustrated uniform distribution of 16 solitons with allowed inter-soliton separations of  $2\pi n/49$  radians; one pair is spaced by  $4 \times 2\pi/49$  instead of  $3 \times 2\pi/49$  radians. Excess power is apparent in the spectrum at mode  $\mu_x = 49$  (highlighted by the red circle in the plot), and we simulate this crystal by phenomenologically reducing the comb-resonator detuning on mode 49 so that the experimental

and simulated spectra agree. The background wave resulting from the constructive interference of the extended waves of the solitons, each having an angular period of  $2\pi/49$ , is visible in the plots of the simulated intensity in Fig. 1.4b and c.

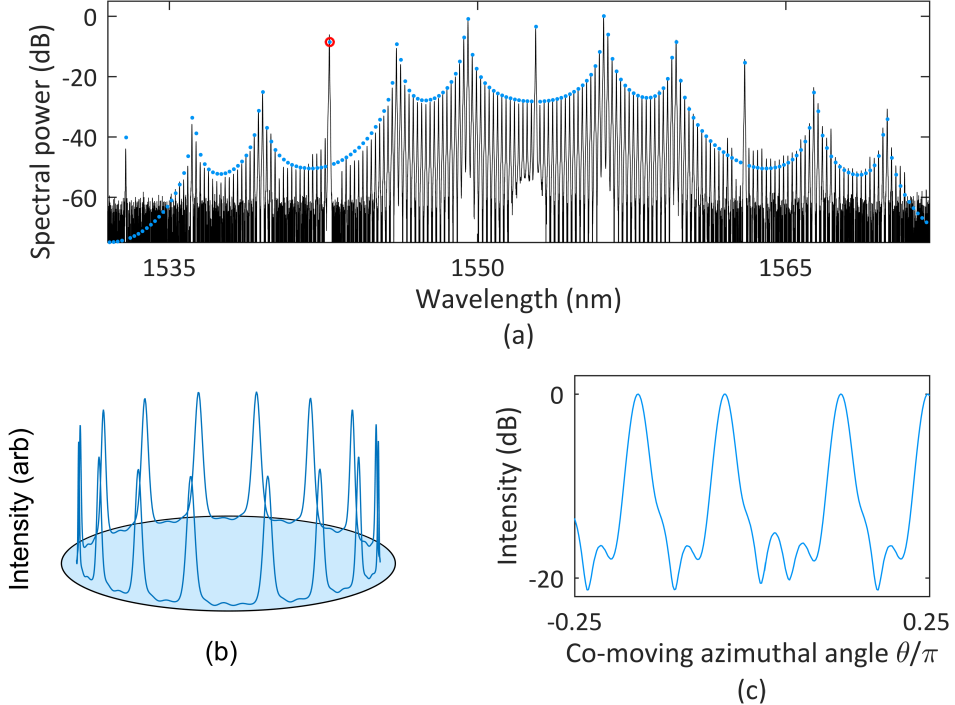


**Figure 1.4: Spectrum and waveform of a superstructured soliton crystal.** (a) Experimental (black) and simulated (blue) optical spectra of a superstructured crystal, with the red dot indicating the location of the mode crossing as described in the text. (b) Simulated time-domain intensity of frustrated-uniform distribution of 16 solitons over 49 lattice points. (c) Zoomed-in logarithm-scale plot of the same that clearly shows unoccupied lattice sites and the anomalous  $4 \times 2\pi/49$  spacing between a pair of pulses.

To gain insight into crystal generation, we simulate laser frequency scans across the resonance that generate this crystal in the presence of the mode crossing on mode 49. Example scans are shown for the case without the mode crossing (green) and with it (blue) in Fig. 2d. In both scans, solitons emerge from chaos as the frequency of the laser is decreased. In the presence of the mode crossing, they are generated with inter-soliton separations of  $2\pi n/49$  radians. A greater number of solitons emerge from chaos in the presence of the mode crossing, and this higher number helps to stabilize the crystal against thermal changes in the experiment. Further, upon continuation of

the simulation, some of the solitons in the scan without the mode crossing interact attractively and pair-annihilate, while the crystallized ensemble resulting from the scan with the mode crossing remains stable indefinitely.

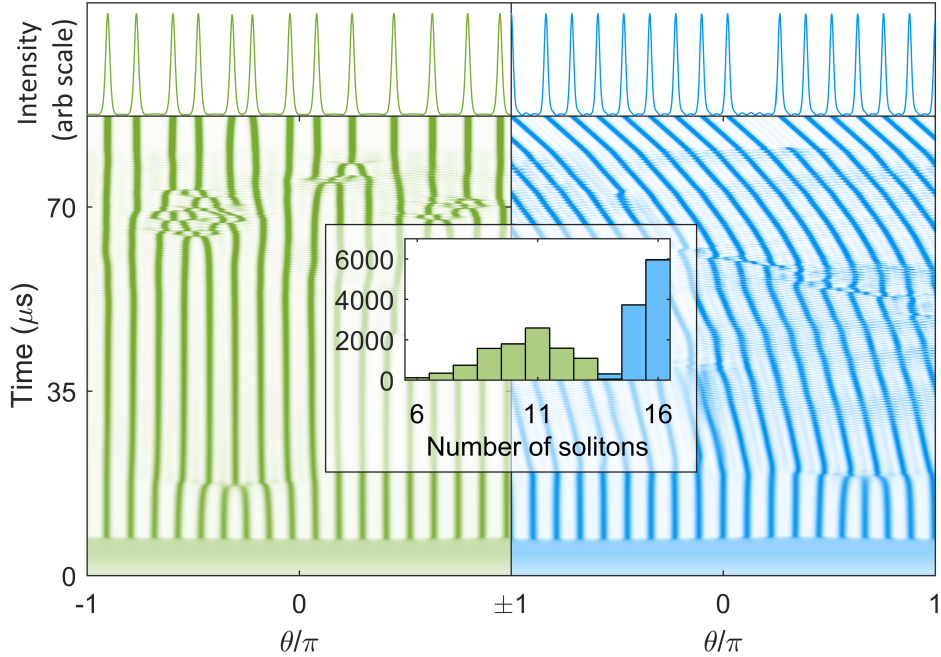


**Figure 1.5: Simulated generation of a superstructured soliton crystal.** Bottom: plots of the intracavity power during a simulated scan across the resonance, without (green) and with (blue) a mode crossing on mode 49 that reduces the comb-resonator detuning and increases the efficiency of frequency conversion on that mode. Top: final waveforms. Inset: histogram of the number of solitons generated in 10,000 simulated scans.

We investigate the pair-distribution function (PDF) for the soliton ensembles generated by these scans. The PDF is the probability that a soliton exists at position  $\theta_0 + \Delta\theta$  given that a different soliton exists at position  $\theta_0$ , normalized to the density. This is a useful metric to classify particle interactions which we borrow from condensed matter physics (see e.g. Ref. [53], especially Fig. 2, and Ref. [54], especially Fig. 1.1 and Chapter 3). We note that for numerically calculated discrete PDFs the absolute scaling of the PDF is not important, as it depends on the density of numerical sampling. In Fig. 2e, we plot the average PDFs for 10000 simulated scans with and without the mode crossing. The result for the case with a mode crossing is sharply peaked, indicating that

the allowed inter-soliton separations take on discrete values. The result for the case without the mode crossing is continuous, with a peak near the most likely nearest-neighbour separation and periodic revivals at its multiples, falling to the value of the PDF for uncorrelated soliton positions (the density) at large separations. This is exactly the expected form of the PDF for a liquid [53, 54]. For comparison, we plot a PDF (black, Fig. 2e) generated by simulation of a simple particle ensemble with mean inter-particle separation of  $\Delta\theta = 0.155\pi$  and normally distributed noise on this value with standard deviation of  $\sigma_{\delta\theta} = 0.18\Delta\theta$ . Thus, with a particle labeled by  $n = 0$  fixed at  $\theta = 0$ , the position of particle  $n$  is  $\theta_0 = n\Delta\theta + \Sigma_n \delta\theta_i$ , with  $\delta\theta_i$  the instantiations of the random variable representing the noise on the pulse spacings.

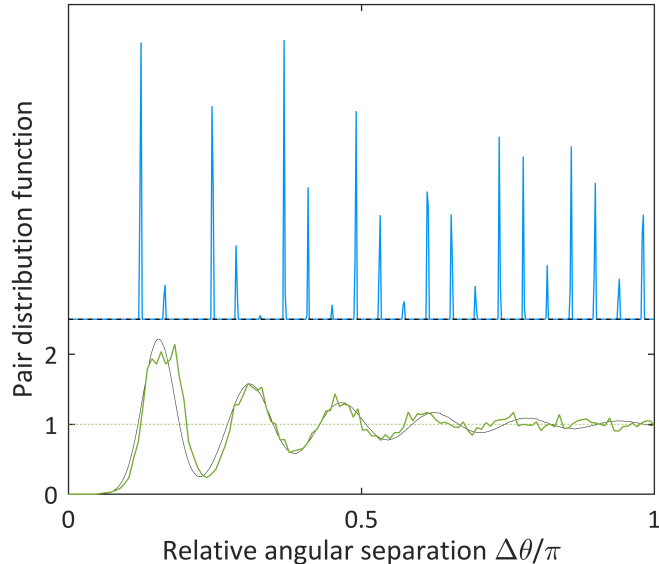


**Figure 1.6: Pair distribution function for soliton crystal generation.** Average pair-distribution functions calculated over 10,000 simulated scans across the resonance with (blue) and without (green) a mode crossing on mode 49. The width of the peaks in the discrete PDF is a single  $\Delta\theta$  bin. The expected PDF of a simple one-dimensional liquid (see main text) is plotted for comparison in black.

## 1.5 Soliton crystal configuration space

We observe a rich variety of soliton crystals explained by ordering in accordance with an extended background wave as described above. Operationally, we adjust the pump laser power to

provide repeatable conditions for creating particular crystals; crystals exhibiting a greater number and variety of defects occur with increased laser power, which intensifies the fluctuations in the chaos that precedes crystal generation and provides less well-ordered initial conditions. Once a crystal is generated, it is stable to small adjustments in the pump power and detuning in accordance with the range of soliton existence shown in Fig. ??, as the crystal structure is determined by the initial conditions for soliton formation rather than by an explicit dependence on pump power or detuning.

Our interpretation of experimental data is based first on the fact that the LLE restricts the behavior of the field  $\psi$  to either an extended pattern (primary comb pulse train or chaos) or an ensemble of solitons. When measurements indicate that a Kerr-comb simultaneously exhibits 1. A quiet repetition-rate tone when the spectrum of the photodetected power is analyzed, and 2. Single-FSR spacing in the power spectrum, it is likely that this comb is a soliton crystal<sup>2</sup>. To determine the temporal structure of a soliton crystal, we begin with the assumption that the spectrum corresponds to a soliton ensemble. Using the properties of the Fourier transform (e.g. linear superposition and the fact that a shift in time corresponds to a linear spectral phase shift), it is usually possible to deduce the configuration of pulses that must lead to the observed spectrum. Once the pulse train corresponding to the general structure of the spectrum has been deduced, the experimental spectrum can be compared to the spectrum of this pulse train calculated as an ensemble of solitons according to Eq. ???. This comparison reveals localized excess power in the experimental spectrum, which is evidence of a mode crossing. The strength of the mode crossing, controlled in the experiment by e.g. the taper-induced coupling between modes, is determined phenomenologically from the magnitude of the excess power and reduced comb-resonator detuning on a single optical mode is incorporated into a perturbed LLE as described in Sec. 1.3. It is then verified that the pulse train whose spectrum matches the experimental data is a steady-state solution to this perturbed LLE, which requires the inter-soliton separations to be multiples of the period of the beat between the excess power and the pump laser. This period is  $2\pi/\mu_x$ , where  $\mu_x$  is the mode number of the effected mode. Because this

---

<sup>2</sup> These requirements are probably sufficient, but not necessary—for example, a defect-free crystal will exhibit multi-FSR spacing. Experimentally, the difference between such a crystal and a primary-comb pulse train lies in the parameters  $\alpha$  and  $F^2$  that place the pump laser *either* in the regime for solitons or the regime for primary comb. However, these are not necessarily straightforward to determine.

process connects the presence of excess power on a single optical mode of the Kerr-comb spectrum to the general shape of the spectrum, two observations that are not related a priori, it provides strong evidence that the time-domain waveform of the crystal has been determined correctly.

The crystals we observe exhibit vacancies (Schottky defects), dislocations (Frenkel defects), disorder, or superstructure, or some combination thereof [55]. Disordered crystals are crystals in which the solitons fall on the peaks of the extended background wave, but their distribution across these peaks varies without any apparent regular order or favored period. In a disordered crystal, the solitons still occupy lattice sites whose positions are determined by an avoided mode crossing in the resonator spectrum, but their distribution over these lattice sites varies without any apparent regular order or favored period. In this case, it is less straightforward to determine the pulse configuration from the shape of the spectrum. Instead, to determine the pulse configuration for a disordered crystal, we first identify excess power due to a mode crossing through observation of an asymmetry in the spectrum about the pump. The location of the excess power then fixes the allowed inter-soliton separations in the resonator, after which an exhaustive search is performed until a pulse train is found that yields the experimental spectrum.

Optical spectra for various observed and hypothetical soliton crystals are plotted in Fig. 1.7. We have simulated 13 of the experimental spectra as steady-state solutions to a perturbed LLE (this excludes crystal o); for 10 of these, the stabilizing mode crossing is visible in the data but not necessarily shown in the figure. For the other three the position of the mode crossing is inferred from the distribution of solitons and other crystal states observed in the same resonator.

We highlight the crystal plotted in Fig. 1.7n. This crystal exhibits both superstructure, with a superlattice period of  $2\pi/3$  radians, and a Frenkel defect. Three identical supercells per resonator round-trip yield a spectrum which has light in optical modes spaced by three resonator FSR, because the waveform's period has been reduced threefold. The Frenkel defect, occurring once per round-trip, contributes the single-FSR lobes to the spectrum. The result is three bursts of pulses containing 8, 9, and 10 solitons respectively.

Fig. 1.7o shows a soliton crystal with inter-soliton separations that are slightly irregular and

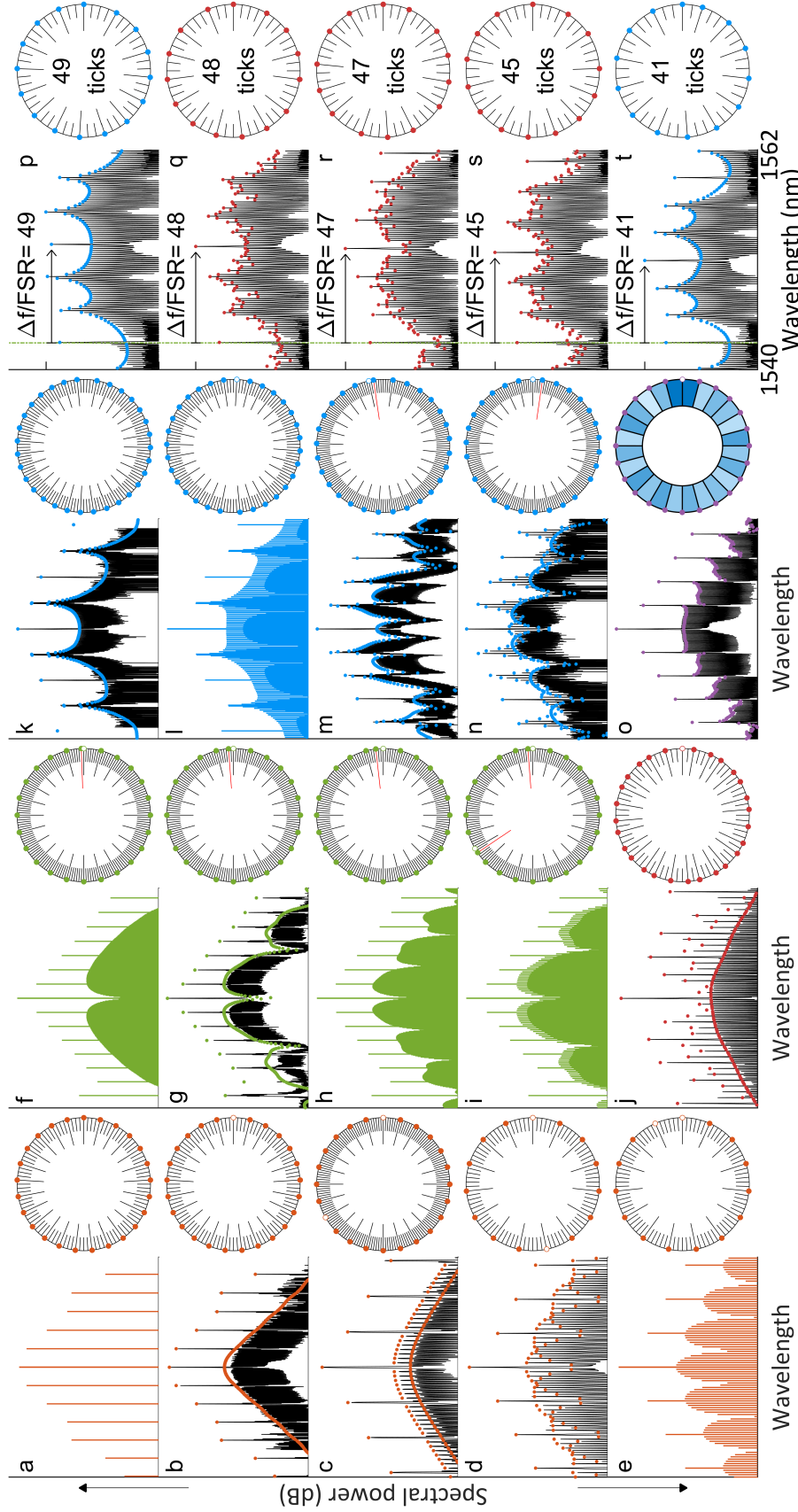


**Figure 1.7: Taxonomy of soliton crystals.** Measured optical spectra are shown in black, with simulations in color. Schematic depictions of the soliton distribution in the resonator co-moving frame are shown to the right of each spectrum. Major ticks in the schematic diagrams indicate the location or expected location of a soliton. Minor ticks indicate lattice sites, corresponding to peaks of the extended background wave due to a mode crossing. (a-e) Soliton crystals exhibiting vacancies. (f-i) Soliton crystals exhibiting superstructure. (j) A disordered crystal. (k-n) Crystals with irregular inter-soliton spacings. Darker shading indicates a smaller inter-soliton spacing. The range is inter-soliton spacings in 3 % of the mean. (p-t) A series of crystals generated as the pump laser is moved progressively closer to the stabilizing mode crossing.

which we have not simulated as a steady-state solution of any perturbed LLE. We expect that the formation of the crystal and the distribution of solitons are dictated by mode interactions, but that in this case our simple approximation of a perturbation to the LLE by a reduced comb-resonator detuning on a single comb mode is not appropriate.

Finally, we highlight the series of crystals plotted in Figs. 1.7p-1.7t. This series of crystals was generated by moving the pump laser closer to a mode-crossing in steps of integer multiples of the resonator FSR. This data demonstrates the influence of the background beating between the pump laser and the mode crossing in determining the configuration of solitons in the resonator.

### **1.6 Time-domain measurements of soliton crystals**

It is recognized in ultrafast optics that it is not generally possible to infer the time-domain waveform of an optical signal from its optical power spectrum without additional information [56], because the spectrum contains no phase information. The LLE imposes restrictions on the possible time-domain field behaviors that can be exhibited, which can allow educated guesses to be made about the time-domain field based on the recorded optical spectrum. However, it is useful to confirm the LLE-assisted interpretation of experimental data both to strengthen the case for the LLE as a useful model for the system and to stay alert to the possibility of extra-LLE phenomena.

To verify our time-domain interpretation of the soliton-crystal spectra we record in experiment, we characterize the temporal intensity of a crystal using an optical cross-correlation measurement. A depiction of the approach and the results for measurement of the time-domain intensity of crystal (j) shown in Fig. 1.7 is shown in Fig. 1.8. We send the Kerr-comb output and an optical reference pulse train through a LiIO<sub>3</sub> crystal with a relative angle of 90° between the beams. When the beams overlap in the crystal an amount of light proportional to the product of their intensities, at the sum of their frequencies, is emitted in a third direction. By measuring the average power of this emitted light while scanning the relative delay between the two beams, we measure the intensity cross-correlation between the crystal and the reference pulse.

In the limit of a delta-function reference pulse, optical cross-correlation directly measures the

time-domain waveform of an unknown signal. To approximate this limit, we perform cross-correlation measurements with a train of reference pulses with duration comparable to that of the solitons, which allows us to precisely characterize the crystal. The reference pulse train is derived through electro-optic modulation (see Chapter ??) from the same laser that pumps the resonator that generates the crystal, and the repetition rate of the reference pulse train is locked to the repetition rate of the Kerr-comb output.

The crystal is generated in a through-coupled configuration, which results in interference between the out-coupled solitons and the through-coupled pump that depends on the coupling condition and that effects the time-domain waveform that propagates away from the resonator. In this particular experiment the out-coupled solitons destructively interfere with the through-coupled pump, with the result that the solitons manifest as dips in the through-coupled intensity. To correct this, before cross-correlation we use a spatial light modulator to rotate the phase of the pump laser by  $\pi$  so that it constructively interferes with the solitons, yielding solitons riding on top of a CW background.

The cross-correlation of crystal (j) with the reference pulse train confirms our interpretation of the spectral data for this crystal. Fig. 1.8b shows the simulated time-domain waveforms of the reference pulse and the crystal, and Fig. 1.8 shows the measured and simulated cross-correlation signals. The temporal spacing between the peaks of the cross-correlation signals is shown in Fig. 1.8, where a high degree of agreement between the data and the simulation is observed.

The simulated cross-correlation signal is sensitive to the intensity profile of the reference pulse. We can measure only its intensity autocorrelation, which we combine with our knowledge of its production to estimate the intensity profile. To demonstrate that the validity of the results we present here is not sensitive to the exact assumptions we make about the intensity profile, we have also simulated the intensity cross-correlation resulting from an assumed Gaussian reference pulse with the same autocorrelation width as is measured for the reference pulse. The resulting simulated cross-correlation does not qualitatively agree as well with the experimental data in the depths of the wells between peaks because it does not contain satellite pulses which contribute to the variations in

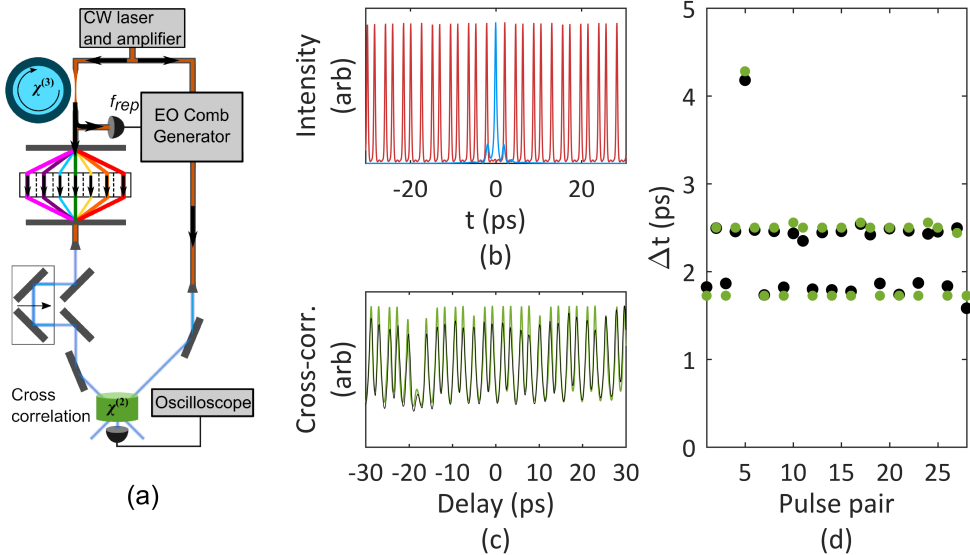


**Figure 1.8: Cross-correlation characterization of a soliton crystal.** Schematic depiction of the setup for using an electro-optic (EO) modulator comb as a reference pulse to measure the time-domain waveform of a soliton crystal. The  $\chi^{(3)}$  (Kerr) and  $\chi^{(2)}$  nonlinearities are indicated on the resonator and nonlinear crystal (LiIO<sub>3</sub>). A spatial light modulator is used to rotate the phase of the pump laser by  $\pi$  after crystal generation to compensate for interference between the out-coupled soliton crystal and the through-coupled pump light. The soliton crystal and the EO modulator comb share a pump laser, and the repetition frequency  $f_{rep}$  of the EOM comb is locked to that of the crystal. Varying the relative delay in one arm of this interferometer enables measurement of the intensity cross-correlation between the soliton crystal and the reference pulse. (b) Simulated crystal (red) and reference (blue) intensity profiles. (c) Measured (black) and simulated (green) cross-correlation signals. The contrast between peaks of the cross-correlation signal, for both theory and experiment, is limited by the duration and shape of the reference pulse and increases between soliton pairs with larger temporal separations. (d) Temporal separations between adjacent peaks for the measured (black) and simulated (green) cross-correlation signals. Mean fractional error is 3.5 %.

this depth, but the quantitative comparison of the temporal spacing between peaks is similar: the mean (maximum) normalized error between experiment and theory is 3.5 % (9.1 %) for the assumed electro-optic comb pulse and 4.8 % (10.6 %) for the Gaussian pulse.

could add a figure showing this

## References

- [1] E. Obrzud, S. Lecomte, and T. Herr. Temporal solitons in microresonators driven by optical pulses. *Nature Photonics*, 11 (August), **2017**, 600–607. DOI: [10.1038/nphoton.2017.140](https://doi.org/10.1038/nphoton.2017.140). arXiv: [1612.08993](https://arxiv.org/abs/1612.08993).
- [2] P. Del'Haye, S. A. Diddams, and S. B. Papp. Laser-machined ultra-high-Q microrod resonators for nonlinear optics. *Applied Physics Letters*, 102, **2013**, 221119 (cited on page 1).
- [3] A. N. Oraevsky. Whispering-gallery waves. *Quantum Electronics*, 32 (42), **2002**, 377–400. DOI: [10.1070/QE2001v031n05ABEH002205](https://doi.org/10.1070/QE2001v031n05ABEH002205). arXiv: [arXiv:1011.1669v3](https://arxiv.org/abs/1011.1669v3).
- [4] H. A. Haus. **Waves and Fields in Optoelectronics**. Englewood Cliffs: Prentice-Hall, 1984.
- [5] S. M. Spillane, T. J. Kippenberg, O. J. Painter, and K. J. Vahala. Ideality in a Fiber-Taper-Coupled Microresonator System for Application to Cavity Quantum Electrodynamics. *Physical review letters*, 91 (4), **2003**, 043902. DOI: [10.1103/PhysRevLett.91.043902](https://doi.org/10.1103/PhysRevLett.91.043902).
- [6] V. S. Il'chenko and M. L. Gorodetskii. Thermal nonlinear effects in optical whispering gallery microresonators.pdf. *Laser Physics*, 2 (6), **1992**, 1004–1009.
- [7] T. Carmon, L. Yang, and K. J. Vahala. Dynamical thermal behavior and thermal self-stability of microcavities. *Optics Express*, 12 (20), **2004**, 4742–4750. URL: <http://www.ncbi.nlm.nih.gov/pubmed/19484026> <http://www.opticsinfobase.org/oe/abstract.cfm?uri=oe-12-20-4742>.
- [8] R. W. Boyd. **Nonlinear Optics**. San Diego, CA: Elsevier, 2003.
- [9] G. P. Agrawal. **Nonlinear Fiber Optics**. 4th. Burlington, MA: Elsevier, 2007.
- [10] R. del Coso and J. Solis. Relation between nonlinear refractive index and third-order susceptibility in absorbing media. *Journal of the Optical Society of America B*, 21 (3), **2004**, 640. DOI: [10.1364/JOSAB.21.000640](https://doi.org/10.1364/JOSAB.21.000640).
- [11] P. Del'Haye, A. Schliesser, O. Arcizet, T. Wilken, R. Holzwarth, and T. J. Kippenberg. Optical frequency comb generation from a monolithic microresonator. *Nature*, 450 (7173), **2007**, 1214–1217. DOI: [10.1038/nature06401](https://doi.org/10.1038/nature06401).
- [12] T. Kippenberg, S. Spillane, and K. Vahala. Kerr-Nonlinearity Optical Parametric Oscillation in an Ultrahigh-Q Toroid Microcavity. *Physical Review Letters*, 93 (8), **2004**, 083904. DOI: [10.1103/PhysRevLett.93.083904](https://doi.org/10.1103/PhysRevLett.93.083904).

- [13] A. A. Savchenkov, A. B. Matsko, D. Strekalov, M. Mohageg, V. S. Ilchenko, and L. Maleki. Low threshold optical oscillations in a whispering gallery mode CaF<sub>2</sub> resonator. *Physical Review Letters*, 93 (24), **2004**, 2–5. DOI: 10.1103/PhysRevLett.93.243905.
- [14] I. H. Agha, Y. Okawachi, M. A. Foster, J. E. Sharping, and A. L. Gaeta. Four-wave-mixing parametric oscillations in dispersion-compensated high- Q silica microspheres. *Physical Review A - Atomic, Molecular, and Optical Physics*, 76 (4), **2007**, 1–4. DOI: 10.1103/PhysRevA.76.043837.
- [15] F. Leo, S. Coen, P. Kockaert, S.-P. Gorza, P. Emplit, and M. Haelterman. Temporal cavity solitons in one-dimensional Kerr media as bits in an all-optical buffer. *Nature Photonics*, 4 (7), **2010**, 471–476. DOI: 10.1038/nphoton.2010.120.
- [16] T. Herr, K. Hartinger, J. Riemensberger, C. Y. Wang, E. Gavartin, R. Holzwarth, M. L. Gorodetsky, and T. J. Kippenberg. Universal formation dynamics and noise of Kerr-frequency combs in microresonators. *Nature Photonics*, 6 (7), **2012**, 480–487. DOI: 10.1038/nphoton.2012.127.
- [17] Y. K. Chembo and C. R. Menyuk. Spatiotemporal Lugiato-Lefever formalism for Kerr-comb generation in whispering-gallery-mode resonators. *Physical Review A*, 87, **2013**, 053852. DOI: 10.1103/PhysRevA.87.053852.
- [18] S. Coen, H. G. Randle, T. Sylvestre, and M. Erkintalo. Modeling of octave-spanning Kerr frequency combs using a generalized mean-field Lugiato-Lefever model. *Optics letters*, 38 (1), **2013**, 37–39. URL: <http://www.ncbi.nlm.nih.gov/pubmed/23282830>.
- [19] M. Haelterman, S. Trillo, and S. Wabnitz. Dissipative modulation instability in a nonlinear dispersive ring cavity. *Optics Communications*, 91 (5-6), **1992**, 401–407. DOI: 10.1016/0030-4018(92)90367-Z.
- [20] T Hansson, M Bernard, and S Wabnitz. Modulational Instability of Nonlinear Polarization Mode Coupling in Microresonators. 35 (4), **2018**. URL: <https://arxiv.org/pdf/1802.04535.pdf>. arXiv: arXiv:1802.04535v1.
- [21] T. Herr, V. Brasch, J. D. Jost, C. Y. Wang, N. M. Kondratiev, M. L. Gorodetsky, and T. J. Kippenberg. Temporal solitons in optical microresonators. *Nature Photonics*, 8 (2), **2014**, 145–152. DOI: 10.1109/CLEOE-IQEC.2013.6801769. arXiv: 1211.0733.
- [22] Y. K. Chembo, I. S. Grudinin, and N Yu. Spatiotemporal dynamics of Kerr-Raman optical frequency combs. *Physical Review A*, 92 (4), **2015**, 4. DOI: 10.1103/PhysRevA.92.043818.
- [23] C. Godey, I. V. Balakireva, A. Coillet, and Y. K. Chembo. Stability analysis of the spatiotemporal Lugiato-Lefever model for Kerr optical frequency combs in the anomalous and normal dispersion regimes. *Physical Review A*, 89 (6), **2014**, 063814. DOI: 10.1103/PhysRevA.89.063814.
- [24] I. V. Barashenkov and Y. S. Smirnov. Existence and stability chart for the ac-driven, damped nonlinear Schrödinger solitons. *Physical Review E - Statistical Physics, Plasmas, Fluids, and Related Interdisciplinary Topics*, 54 (5), **1996**, 5707–5725. DOI: 10.1103/PhysRevE.54.5707.

- [25] A Coillet and Y. K. Chembo. Routes to spatiotemporal chaos in Kerr optical frequency combs. *Chaos*, 24 (1), **2014**, 5. doi: 10.1063/1.4863298. arXiv: arXiv:1401.0927v1.
- [26] L. A. Lugiato and R Lefever. Spatial Dissipative Structures in Passive Optical Systems. *Physical Review Letters*, 58 (21), **1987**, 2209–2211.
- [27] L. Lugiato and R Lefever. Diffraction stationary patterns in passive optical systems. *Interaction of Radiation with Matter*, **1987**.
- [28] W. H. Renninger and P. T. Rakich. Closed-form solutions and scaling laws for Kerr frequency combs. *Scientific Reports*, 6 (1), **2016**, 24742. doi: 10.1038/srep24742. arXiv: 1412.4164.
- [29] X. Yi, Q.-F. Yang, K. Y. Yang, M.-G. Suh, and K. Vahala. Soliton frequency comb at microwave rates in a high-Q silica microresonator. *Optica*, 2 (12), **2015**, 1078–1085 (cited on page 5).
- [30] S. Coen and M. Erkintalo. Universal scaling laws of Kerr frequency combs. *Optics letters*, 38 (11), **2013**, 1790–1792. doi: 10.1364/OL.38.001790. arXiv: arXiv:1303.7078v1.
- [31] V. Brasch, T. Herr, M. Geiselmann, G. Lihachev, M. H. P. Pfeiffer, M. L. Gorodetsky, and T. J. Kippenberg. Photonic chip-based optical frequency comb using soliton Cherenkov radiation. *Science*, 351 (6271), **2016**, 357. doi: 10.1364/CLEO\_SI.2015.STh4N.1. arXiv: 1410.8598.
- [32] V. E. Lobanov, G. V. Lihachev, N. G. Pavlov, A. V. Cherenkov, T. J. Kippenberg, and M. L. Gorodetsky. Harmonization of chaos into a soliton in Kerr frequency combs. *Optics Express*, 24 (24), **2016**, 27382. doi: 10.1126/science.aah4243. arXiv: 1607.08222.
- [33] J. K. Jang, M. Erkintalo, S. G. Murdoch, and S. Coen. Writing and erasing of temporal cavity solitons by direct phase modulation of the cavity driving field. *Optics Letters*, 40 (20), **2015**, 4755–4758. doi: 10.1364/OL.40.004755. arXiv: 1501.05289.
- [34] J. K. Jang, M. Erkintalo, S. Coen, and S. G. Murdoch. Temporal tweezing of light through the trapping and manipulation of temporal cavity solitons. *Nature Communications*, 6, **2015**, 7370. doi: 10.1038/ncomms8370. arXiv: 1410.4836.
- [35] Y. Wang, B. Garbin, F. Leo, S. Coen, M. Erkintalo, and S. G. Murdoch. Writing and Erasure of Temporal Cavity Solitons via Intensity Modulation of the Cavity Driving Field. *arXiv*, **2018**, 1802.07428. arXiv: 1802.07428.
- [36] H. Taheri, A. A. Eftekhar, K. Wiesenfeld, and A. Adibi. Soliton formation in whispering-gallery-mode resonators via input phase modulation. *IEEE Photonics Journal*, 7 (2), **2015**, 2200309. doi: 10.1109/JPHOT.2015.2416121.
- [37] S. B. Papp, K. Beha, P. Del'Haye, F. Quinlan, H. Lee, K. J. Vahala, and S. A. Diddams. Microresonator frequency comb optical clock. *Optica*, 1 (1), **2014**, 10–14. doi: 10.1364/OPTICA.1.000010. arXiv: 1309.3525.

- [38] D. T. Spencer, T. Drake, T. C. Briles, J. Stone, L. C. Sinclair, C. Fredrick, Q. Li, D. Westly, B. R. Ilic, A. Bluestone, N. Volet, T. Komljenovic, L. Chang, S. H. Lee, D. Y. Oh, T. J. Kippenberg, E. Norberg, L. Theogarajan, M.-g. Suh, K. Y. Yang, H. P. Martin, K. Vahala, N. R. Newbury, K. Srinivasan, J. E. Bowers, S. A. Diddams, and S. B. Papp. An optical-frequency synthesizer using integrated photonics. *Nature*, 557, **2018**, 81–85. DOI: 10.1038/s41586-018-0065-7.
- [39] H. Lee, T. Chen, J. Li, K. Y. Yang, S. Jeon, O. Painter, and K. J. Vahala. Chemically etched ultrahigh-Q wedge-resonator on a silicon chip. *Nature Photonics*, 6 (6), **2012**, 369–373. DOI: 10.1038/nphoton.2012.109. arXiv: 1112.2196 (cited on page 1).
- [40] M. Zajnulina, M. Böhm, D. Bodenmüller, K. Blow, J. C. Boggio, A. Rieznik, and M. Roth. Characteristics and stability of soliton crystals in optical fibres for the purpose of optical frequency comb generation. *Optics Communications*, 393 (November 2016), **2017**, 95–102. DOI: 10.1016/j.optcom.2017.02.035 (cited on page 1).
- [41] A. Haboucha, H. Leblond, M. Salhi, A. Komarov, and F. Sanchez. Coherent soliton pattern formation in a fiber laser. *Optics Letters*, 33 (5), **2008**, 524–526. DOI: 10.1364/OL.33.000524 (cited on page 1).
- [42] F. Amrani, M. Salhi, P. Grelu, H. Leblond, and F. Sanchez. Universal soliton pattern formations in passively mode-locked fiber lasers. *Optics letters*, 36 (9), **2011**, 1545–1547. DOI: 10.1364/OL.36.001545 (cited on page 1).
- [43] A. Haboucha, H. Leblond, M. Salhi, A. Komarov, and F. Sanchez. Analysis of soliton pattern formation in passively mode-locked fiber lasers. *Physical Review A*, 78, **2008**, 043806. DOI: 10.1103/PhysRevA.78.043806 (cited on page 1).
- [44] B. A. Malomed, A Schwache, and F Mitschke. Soliton lattice and gas in passive fiber-ring resonators. *Fiber and Integrated Optics*, 17 (4), **1998**, 267–277. DOI: 10.1080/014680398244867 (cited on page 1).
- [45] F. Mitschke and A. Schwache. Soliton ensembles in a nonlinear resonator. *Journal of Optics B: Quantum and Semiclassical Optics*, 10 (6), **1998**, 779–788 (cited on page 1).
- [46] A. Schwache and F. Mitschke. Properties of an optical soliton gas. *Physical Review E*, 55 (6), **1997**, 7720–7725. DOI: 10.1103/PhysRevE.55.7720 (cited on page 1).
- [47] H. A. Haus and W. Huang. Coupled-Mode Theory. *Proceedings of the IEEE*, 79 (10), **1991**, 1505–1518. DOI: 10.1109/5.104225 (cited on pages 4, 7).
- [48] T. Herr, V. Brasch, J. D. Jost, I. Mirgorodskiy, G. Lihachev, M. L. Gorodetsky, and T. J. Kippenberg. Mode Spectrum and Temporal Soliton Formation in Optical Microresonators. *Physical Review Letters*, 113 (12), **2014**, 123901. DOI: 10.1103/PhysRevLett.113.123901 (cited on page 5).
- [49] Y. Liu, Y. Xuan, X. Xue, P.-H. Wang, S. Chen, A. J. Metcalf, J. Wang, D. E. Leaird, M. Qi, and A. M. Weiner. Investigation of mode coupling in normal-dispersion silicon nitride microresonators for Kerr frequency comb generation. *Optica*, 1 (3), **2014**, 137–144. DOI: 10.1364/OPTICA.1.000137 (cited on page 6).

- [50] T. Hansson and S. Wabnitz. Bichromatically pumped microresonator frequency combs. *Physical Review A*, 90, **2014**, 013811. DOI: 10.1103/PhysRevA.90.013811. arXiv: 1404.2792 (cited on page 6).
- [51] D. V. Skryabin and W. J. Firth. Interaction of cavity solitons in degenerate optical parametric oscillators. *Optics letters*, 24 (15), **1999**, 1056–1058. DOI: 10.1364/OL.24.001056. arXiv: 9906004 [patt-sol] (cited on page 6).
- [52] S. Wabnitz. Control of soliton train transmission, storage, and clock recovery by cw light injection. *Journal of the Optical Society of America B*, 13 (12), **1996**, 2739–2749. URL: <http://www.scopus.com/inward/record.url?eid=2-s2.0-0030378988&partnerID=tZ0tx3y1> (cited on page 6).
- [53] J. A. Barker and D. Henderson. What is "liquid"? Understanding the states of matter. *Reviews of Modern Physics*, 48 (4), **1976**, 587–671. DOI: 10.1103/RevModPhys.48.587 (cited on pages 10, 11).
- [54] T. Egami and S. Billinge. **Underneath the Bragg Peaks**. 2nd. Oxford, UK: Elsevier, 2012, p. 422 (cited on pages 10, 11).
- [55] N. W. Ashcroft and D. N. Mermin. **Solid State Physics**. 1st ed. Belmont, CA: Brooks/Cole, 1976, p. 826 (cited on page 13).
- [56] A. Weiner. **Ultrafast Optics**. 1st ed. Hoboken, NJ: Wiley, 2009, p. 598 (cited on page 15).